The iterative thermal emission method: A more implicit modification of IMC

Citation	Long, A. R., Gentile, N. A., & Palmer, T. S. (2014). The iterative thermal emission method: A more implicit modification of IMC. Journal of Computational Physics, 277, 228-247. doi:10.1016/j.jcp.2014.08.017
DOI	10.1016/j.jcp.2014.08.017
Publisher	Elsevier
Version	Version of Record
Terms of Use	http://cdss.library.oregonstate.edu/sa-termsofuse

Journal of Computational Physics 277 (2014) 228–247

Contents lists available at ScienceDirect

Journal of Computational Physics

www.elsevier.com/locate/jcp

The iterative thermal emission method: A more implicit modification of IMC

A.R. Long [a,*], N.A. Gentile [b], T.S. Palmer [c]

[a] Department of Nuclear Engineering, Texas A&M University, 3133 TAMU, College Station, TX 77843, USA
[b] Lawrence Livermore National Laboratory, L-38, P.O. Box 808, Livermore, CA 94550, USA
[c] Nuclear Engineering and Radiation Health Physics, Oregon State University, 100 Radiation Center, Corvallis, OR 97333, USA

ARTICLE INFO

Article history:
Received 10 February 2013
Received in revised form 5 August 2014
Accepted 10 August 2014
Available online 19 August 2014

Keywords:
Thermal radiative transfer
Implicit Monte Carlo

ABSTRACT

For over 40 years, the Implicit Monte Carlo (IMC) method has been used to solve challenging problems in thermal radiative transfer. These problems typically contain regions that are optically thick and diffusive, as a consequence of the high degree of "pseudo-scattering" introduced to model the absorption and reemission of photons from a tightly-coupled, radiating material. IMC has several well-known features that could be improved: a) it can be prohibitively computationally expensive, b) it introduces statistical noise into the material and radiation temperatures, which may be problematic in multiphysics simulations, and c) under certain conditions, solutions can be nonphysical, in that they violate a *maximum principle*, where IMC-calculated temperatures can be greater than the maximum temperature used to drive the problem.

We have developed a variant of IMC called *iterative thermal emission* IMC, which is designed to have a reduced parameter space in which the maximum principle is violated. ITE IMC is a more implicit version of IMC in that it uses the information obtained from a series of IMC photon histories to improve the estimate for the end of time step material temperature during a time step. A better estimate of the end of time step material temperature allows for a more implicit estimate of other temperature-dependent quantities: opacity, heat capacity, Fleck factor (probability that a photon absorbed during a time step is not reemitted) and the Planckian emission source.

We have verified the ITE IMC method against 0-D and 1-D analytic solutions and problems from the literature. These results are compared with traditional IMC. We perform an infinite medium stability analysis of ITE IMC and show that it is slightly more numerically stable than traditional IMC. We find that significantly larger time steps can be used with ITE IMC without violating the maximum principle, especially in problems with non-linear material properties. The ITE IMC method does however yield solutions with larger variance because each sub-step uses a different Fleck factor (even at equilibrium).

1. Introduction

Thermal radiative transfer (TRT) is an integral part of many high energy density physics problems [1–3]. One standard approach for simulating TRT is the Implicit Monte Carlo method developed by Fleck and Cummings [4]. A drawback of the IMC

* Corresponding author.
E-mail address: arlong.ne@tamu.edu (A.R. Long).

http://dx.doi.org/10.1016/j.jcp.2014.08.017
0021-9991/

method is that time steps must be sufficiently small in cases where the material is heated by a radiation field. If the time step is too large, the material will absorb too much energy and reach a nonphysically high temperature, which is a violation of the *maximum principle* [5]. In problems where a material temperature source is used as the boundary condition, this means that the matter inside the problem will reach a higher temperature than the boundary heat source for the problem. Another issue in the IMC method arises from treating the material temperature as uniform within a spatial cell. This leads to a problem known as *teleportation error*, where particle absorptions may occur in some small fraction of a cell, but the emission on the next time step is uniform within the cell. Thus, particles are emitted ahead of where physical heating has occurred, and in some cases, energy travels faster than the speed of light. Methods exist to ameliorate teleportation error, but they are beyond the scope of this paper [6].

The violation of the maximum principle is nonphysical and several attempts have been made to correct it by modifying the form of the IMC Fleck factor [7–9] and by using predictor–corrector approaches for the temperature or material properties [7,6]. Another area of research is the prediction of conditions under which maximum principle violations will occur in IMC [10]. The disadvantage of modifying the Fleck factor is that its constituent variables are still explicitly dependent on the temperature of the material at the beginning of the time step. Predictor–corrector methods use a fraction of the particle histories to estimate the temperature at the next time step and use this information to update material properties. This method can be effective in reducing violations in the maximum principle, but it requires a predictive step which may be computationally expensive. In this paper we modify the IMC equations so that a single time step can be subdivided into a user-determined number of sub-steps. These sub-steps do not represent a temporal splitting of the time step, but rather a splitting of the total energy in the problem at each time step. The equations for each sub-step are solved in turn by performing an IMC simulation with a slightly modified Fleck factor. After a sub-step simulation is completed, the information from that sub-step is used to obtain a better estimate for the material temperature at the end of the time step. This material temperature is then used to update the thermal emission source and the temperature-dependent material properties. After all the sub-steps are completed, the final temperature is determined and the same process is used on the next time step. We call this method the Iterative Thermal Emission Implicit Monte Carlo method (ITE IMC). The ITE IMC method is similar to predictor–corrector methods in that we use particle histories to treat parameters more implicitly, but every particle history is also used to determine the material temperature at the end of the time step.

The remainder of this paper will be organized as follows: in Section 2, the Implicit Monte Carlo equations are derived using a Taylor series expansion in temperature. The ITE IMC equations are then derived in Section 3 by splitting the material temperature into sub-steps and manipulating Taylor series expansions. In Section 4, the results of calculations using the ITE IMC method are compared to those of the IMC method and analytic solutions for common TRT test problems. Section 4 also includes a 0-D stability analysis for the ITE IMC method. In Section 5, the parameter space for maximum principle violations is explored for the IMC and ITE IMC methods, and the variance and teleportation error for both methods are compared.

2. Implicit Monte Carlo

The thermal radiative transfer equations are non-linear in material energy density. The standard TRT equations, without scattering and with functional parameters suppressed, are:

$$\frac{1}{c}\frac{\partial I}{\partial t} + \Omega \cdot \nabla I + \sigma_a I = \frac{1}{4\pi}\sigma_a B + S_r, \tag{1}$$

$$\frac{dU_m}{dt} = \int_0^\infty \int_0^{4\pi} \sigma_a I d\Omega d\nu - \int_0^\infty \sigma_a B d\nu + S_m. \tag{2}$$

The terms in Eqs. (1) and (2) are defined with their functional parameters:

$$\begin{aligned} x &= \text{position} \\ \Omega &= \text{solid angle} \\ T &= \text{material temperature} \\ \nu &= \text{frequency} \\ t &= \text{time} \\ I(x,\Omega,\nu,t) &= \text{radiative intensity} \\ U_m(x,T,t) &= \text{material energy density} \\ \sigma_a(x,\nu,T,t) &= \text{material absorption opacity} \\ B(\nu,T,t) &= \text{Planckian emission} \\ S_r(x,\Omega,\nu,T,t) &= \text{source to the radiation field} \\ S_m(x,T,t) &= \text{material energy source} \\ c &= \text{speed of light} \end{aligned}$$

Eq. (1) represents the radiative energy balance and Eq. (2) represents the material energy balance. The material energy density, U_m satisfies:

$$U_m = \int_0^T c_V(T)dT \tag{3}$$

Another useful quantity is the equilibrium radiative energy density, U_r:

$$U_r = aT^4 \tag{4}$$

The change in U_r produced by a change in U_m is described by β:

$$\beta = \frac{\partial U_r}{\partial U_m} = \frac{\partial U_r}{\partial T}\frac{\partial T}{\partial U_m} = \frac{4a(T)^3}{c_V}, \tag{5}$$

where β^n means that the temperature and heat capacity are at time $t = t^n$.

Eqs. (1) and (2) are coupled by the Planckian emission term B, which is a function of frequency and the material temperature:

$$B(\nu, T) = \frac{2h\nu^3}{c^2}\frac{1}{\exp(\frac{h\nu}{kT}) - 1}. \tag{6}$$

The Planckian is often expressed as a function of the equilibrium radiative energy density, U_r, times a probability density function in frequency at a given temperature:

$$B(\nu, T) = b(\nu, T)acT^4 = b(\nu, T)cU_r, \tag{7}$$

$$\int_0^\infty b(\nu, T)d\nu = 1. \tag{8}$$

In the gray and multigroup formulations the opacity is often averaged over the Planckian spectrum. For the gray case:

$$\sigma_{a,p} = \int_0^\infty \sigma_a(\nu, T)b(\nu, T)d\nu. \tag{9}$$

Substituting Eq. (7) into Eqs. (1) and (2) clarifies the temperature relationship in the TRT equations.

We now derive the IMC equations for the gray case. If the material balance equation is integrated over a time step, Δt, the result can be expressed using average quantities:

$$\frac{U_m^{n+1} - U_m}{\Delta t} = \int_0^{4\pi} \sigma \bar{I}\, d\Omega - \sigma_{a,p}ca\bar{T}^4 \tag{10}$$

The radiative energy balance is discretized by assuming the opacity does not change throughout the time step and that emission term uses a temperature at t^{n+1}.

$$\frac{1}{c}\frac{\partial I}{\partial t} + \Omega \cdot \nabla I + \sigma_a^n I = \frac{1}{4\pi}\sigma_a^n ca\left(T^{n+1}\right)^4. \tag{11}$$

In the IMC method we make a series of approximations to linearize the emission term. In Eq. (10) the opacity is assumed to be constant across the time step and evaluated at T^n. The heat capacity, c_V, is also assumed to be constant over a time step. The average temperature in the emission term is taken to be the temperature at the end of the time step. This changes the material energy density balance to a temperature update equation:

$$\frac{U_m^{n+1} - U_m^n}{\Delta t} \approx c_V^n \frac{T^{n+1} - T^n}{\Delta t} = \int_0^{4\pi} \sigma \bar{I}\, d\Omega - \sigma_{a,p}ca\left(T^{n+1}\right)^4. \tag{12}$$

Eq. (12) clearly shows that the material energy balance equation is non-linear in temperature. To linearize this system of equations, the emission term in Eqs. (10) and (11) is approximated with a Taylor series around the time t^n:

$$c_V^n \frac{T^{n+1} - T^n}{\Delta t} = \int_0^{4\pi} \sigma^n \bar{I}\, d\Omega - \sigma_{a,p}^n ca\left(T^n\right)^4 - \Delta t ca\frac{d\sigma T^4}{dT}\frac{dT}{dt}, \tag{13}$$

$$\frac{1}{c}\frac{\partial I}{\partial t} + \Omega \cdot \nabla I + \sigma_a^n I = \frac{1}{4\pi}\sigma_a^n ca\left(T^n\right)^4 + \frac{1}{4\pi}\Delta t\sigma^n 4ca\left(T^n\right)^3\frac{dT}{dt}. \tag{14}$$

This Taylor series expansion makes the equations semi-implicit in material temperature. The opacity term in Eq. (13) can be pulled out of the derivative because we have assumed that the change in opacity is negligible over a time step; this can be a large source of error because opacity can vary as $\frac{1}{T^3}$ (see Ref. [9] for a treatment of the opacity derivative). If this therm were frequency dependent, $b(\nu, T)$ would also assumed to be constant over the time step, which is akin to assuming that the frequency distribution of thermally emitted photons does not vary significantly with temperature. Removing the opacity term and evaluating the derivative, Eq. (13) becomes:

$$c_V^n \frac{T^{n+1} - T^n}{\Delta t} = \int_0^{4\pi} \sigma^n \bar{I}\, d\Omega - \sigma_{a,p}^n c a \left(T^n\right)^4 - \Delta t \sigma^n 4 c a \left(T^n\right)^3 \frac{dT}{dt}. \tag{15}$$

The material energy balance equation is now linear in T^n.

We can now solve Eq. (15) for $\frac{dT}{dt} = \frac{T^{n+1} - T^n}{\Delta t}$ and insert that expression into Eq. (14). Here an additional approximation is made to Eq. (13): the average intensity, $\bar{I}$, has been replaced with instantaneous intensity, I. This yields the radiative energy balance of the traditional IMC equations:

$$\frac{1}{c}\frac{\partial I}{\partial t} + \Omega \cdot \nabla I + \sigma_a^n I = \frac{1}{4\pi} f \sigma_a^n c U_r^n + \frac{1}{4\pi}(1-f) b^n \left(\int_0^{4\pi} \sigma^n I d\Omega \right) + S_r. \tag{16}$$

Here it is worth noting that the IMC approach differs from other numerical methods based on linearizations. In the IMC method, a Taylor series and other approximations are used to obtain an expression for the emission term at t^{n+1}, but instead of solving the linearized material balance equation for T^{n+1}, the emission term is substituted back into the original equation, Eq. (10). This means that a non-linear equation of state can be used to calculate the temperature from U_m^{n+1}, instead of the heat capacity at t^n as Eq. (12) would suggest. Thus the material energy balance becomes:

$$\frac{U_m^{n+1} - U_m^n}{\Delta t} = f \left(\int_0^{4\pi} \sigma^n \bar{I}\, d\Omega - \sigma_{a,p}^n c U_r^n + S_m \right), \tag{17}$$

Both these equations contain the Fleck factor, f:

$$f = \frac{1}{1 + \Delta t \sigma_{a,p}^n c \beta^n}. \tag{18}$$

2.1. Meaning of the Fleck factor

The Fleck factor ranges between 0 and 1 for all problem parameters. As the time step size approaches infinity, the Fleck factor approaches zero. For very small time steps, the Fleck factor approaches unity. The Fleck factor is often described as the probability that an absorbed photon is not reemitted within a time step. This is evident from the second term on the right hand side of Eq. (16): as f approaches zero, more of the angular intensity, I, will be redistributed in angle and frequency. This physically represents the absorption and reemission of a photon. This term is usually referred to as *effective scattering*, because it looks like a scattering event but is unrelated to a physical scattering cross section. As f approaches unity, the effective scattering term vanishes and only absorptions take place.

In the material energy balance, the Fleck factor decreases the amount of energy absorbed and the amount reemitted and thus the change in temperature. If the Fleck factor is not used, all absorbed energy in the material would remain there throughout the time step—a nonphysical approximation that would lead to an overestimation of material temperature if a large energy source is incident on the material [4]. A smaller Fleck factor increases run-time due to the increased effective scattering probability.

3. Iterative thermal emission IMC

The standard IMC equations are modified by assuming that the material temperature can be divided into equal portions. Combining several semi-implicit steps is similar to the Rosenbrock method [11,12]. The material temperature at T^n is:

$$T^n \equiv T_1^n + T_2^n + \ldots + T_{N-1}^n + T_N^n = N T_1, \tag{19}$$

where a sub-temperature T_i is defined by $T_i = \frac{T}{N}$ for $i = 1, 2, \ldots, N$. The change in the first sub-temperature, T_1, in time-implicit form is:

$$\frac{dT_1}{dt} = F\left(T_1^{n+1}\right) = \frac{1}{N} F\left(T^{n+1}\right). \tag{20}$$

The change in T_1 can be expressed in terms of T because of the relationship in Eq. (19). A Taylor series is used to expand $F(T^{n+1})$ around T^n:

$$\frac{dT_1}{dt} = \frac{1}{N}F\left(T^{n+1}\right) \approx \frac{1}{N}\left(F\left(T^{n}\right) + \frac{dF}{dT}\frac{dT}{dt}\Delta t\right) \approx \frac{1}{N}\left(F\left(T^{n}\right) + \frac{dF}{dT}N\frac{dT_1}{dt}\Delta t\right). \tag{21}$$

In Eq. (21), $N\frac{dT_1}{dt}$ is used to represent the $\frac{dT}{dt}$ term. Eq. (21) resembles standard IMC with a $\frac{1}{N}$ term in front of the emission source. T_1^{n+1} can then be determined from the IMC method using $\frac{1}{N}$ of the emission energy.

Now that T_1^{n+1} has been calculated, it can be used to obtain a better estimate of T^{n+1} when determining all subsequent values of T_i^{n+1}. This more accurate estimate of T^{n+1} is used in the material energy balance for T_2^{n+1}:

$$\begin{aligned}\frac{dT_2}{dt} = \frac{1}{N}F\left(T^{n+1}\right) &\approx \frac{1}{N}\left(F\left(T_1^{n+1} + T_2^{n+1} + (N-2)T_N^{n+1}\right)\right)\\ &\approx \frac{1}{N}\left(F\left(T_1^{n+1} + T_2^{n} + (N-2)T_N^{n}\right) + \frac{dF}{dT}(N-2+1)\frac{dT_2}{dt}\Delta t\right)\end{aligned} \tag{22}$$

In Eq. (22), the total temperature $\frac{dT}{dt}$ is approximated with $(N-2+1)\frac{dT_2}{dt}$. This represents the derivative of all unknown sub-step values (2 through N). Solving Eq. (22) for $\frac{dT_2}{dt}$ yields:

$$\frac{dT_2}{dt} = \frac{1}{N}F\left(T_1^{n+1} + T_2^{n} + (N-2)T_N^{n}\right)\left(1 - \frac{(N-2+1)}{N}\frac{dF}{dT}\left(T_1^{n+1} + T_2^{n} + (N-2)T_N^{n}\right)\Delta t\right)^{-1} \tag{23}$$

This process is continued until T_N^{n+1} is determined, then the sum of all the energy deposited in each sub-step is used with an equation of state to find T^{n+1}. The equation for a given sub-temperature T_i in the ITE IMC method is:

$$\frac{dT_i}{dt} = \frac{1}{N}F(T_{i,N})\left(1 - \frac{N-i+1}{N}\frac{dF}{dT}(T_{i,N})\Delta t\right)^{-1}, \tag{24}$$

where

$$T_{i,N} = \left(\sum_{j=1}^{i-1} T_j^{n+1}\right) + (N-i+1)T_i^{n}. \tag{25}$$

The $T_{i,N}$ term is the current estimate for T^{n+1}.

Substituting Eq. (24) into the radiative energy balance equation results in the standard IMC equations except with a slightly modified Fleck factor:

$$f_i = \frac{1}{1 + \frac{N-i+1}{N}\beta c\sigma\Delta t}. \tag{26}$$

The gray Iterative Thermal Emission IMC equations in slab geometry are:

$$\frac{\partial U_{m,i}}{\partial t} = \sigma_{a,p}\int_{-1}^{1} f_i I_i d\mu + \frac{1}{N}f_i acT_{i,N}^4 + f_i\frac{1}{N}S_m, \tag{27}$$

$$\frac{1}{c}\frac{\partial I_i}{\partial t} + \mu\frac{\partial I_i}{\partial x} + \sigma_{a,p}I_i = \frac{1}{N}\frac{1}{2}\left(\sigma_{a,p}f_i caT_{i,N}^4\right) + \frac{1}{2}\int_{-1}^{1}\sigma_{a,p}(1-f_i)I_i d\mu' + \frac{1}{N}S_r. \tag{28}$$

These equations reduce to the standard IMC equations (Eqs. (16) and (17)) if $N = 1$.

The initial intensity each time step is simulated using what are called "census particles" for both IMC and ITE IMC. These are simulated photons that represent the energy already in the radiation field at the start of the time step. As such their birth time is always at the start of each time step, t^n. At equilibrium, the radiation intensity in the ITE IMC equations for sub-step, i, is:

$$I_i = \frac{1}{2}acT_i^4 = \frac{1}{N}\frac{1}{2}acT^4. \tag{29}$$

At equilibrium, each T_i is equal and thus each sub-step will start with the same census energy at the beginning of a simulation. c_V, σ and f_i are functions of temperature and use the T^{n+1} estimate at each sub-temperature.

After all values of T_i and I_i have been determined by Monte Carlo simulation, the material temperature at the next time step, T^{n+1}, is determined by summing the material update equations for each T_i and I_i:

$$T^{n+1} = T^{n} + \Delta t\left(\sum_{i=1}^{N}\frac{1}{c_v}\int_{-1}^{1} f_i\sigma_{a,i}I_i d\mu - \sum_{i=1}^{N}\frac{1}{N}\frac{f_i}{c_v}\sigma_{a,p,i}acT_i^4\right). \tag{30}$$

3.1. Discussion

Other methods that attempt to make IMC more implicit are now compared to the ITE IMC method. Predictor–corrector methods for IMC calculate the temperature at the next time step with some smaller number of particles and then rerun the problem with more particles and an updated temperature guess. ITE IMC differs from this approach in that all particle histories contribute to the final temperature update for a time step. ITE IMC also differs from predictor corrector in that the temperature at subsequent ITE IMC sub-steps does not look like a fixed-point iteration scheme. Each temperature is a composite of the temperatures calculated during the previous sub-step simulations. Predictor–corrector methods are advantageous in that they can use the updated temperature to achieve second order accuracy but this requires setting the implicitness factor, α, to 0.5 [6]. This can lead to stability issues [13]. Predictor–corrector methods have also been used effectively to implement time-step controls and continuous opacity methods [6]. Recently, an IMC method was formulated by using the BDF-2 time integration scheme on the material energy equations [14]. This method includes information from the start of the previous time-step, t^{n-1}, and has been shown to give correct behavior on a 0-D problem with strongly nonlinear opacity (discussed below). The BDF-2 IMC equations use a more accurate time integration, but they do not improve the estimate of the material temperature at t^{n+1}, which is the crux of predictor corrector methods and the ITE IMC method.

An important feature of the IMC equations is that they conserve energy and are strictly positive. The energy conservation is a result of the matching terms of opposite sign in the radiative energy balance and material energy balance. Losses from radiative energy field are a source to the material energy. The terms also match in ITE IMC equations—the emission from the material energy balance is exactly represented as a source in the angle-integrated radiative energy balance. Eq. (30) shows this conservation of emitted energy and absorbed energy when calculating the material temperature at t^{n+1}. The positivity of the IMC equations comes from the fact that there is a maximum amount of energy that can be radiated during a time step. For the ITE IMC equations, the temperature will be positive if the total emission term is less than the current material energy:

$$\frac{1}{N}\sum_{i=1}^{N}\Delta t f_i \sigma a c T_{i,N}^4 < c_V T \tag{31}$$

If Δt is very large, $\frac{N-i+1}{N}\beta c\sigma\,\Delta t \gg 1$, and the inequality becomes:

$$\frac{1}{N}\sum_{i=1}^{N}\frac{\Delta t \sigma a c T_{i,N}^4}{\frac{N-i+1}{N}\beta c\sigma\,\Delta t} < c_V T \tag{32}$$

Inserting the definition of β and reducing, Eq. (32) becomes:

$$\sum_{i=1}^{N}\frac{T_{i,N}}{4(N-i+1)} < T \tag{33}$$

Eq. (33) shows that for the IMC case of $N = 1$, the maximum amount of energy loss through emission is one fourth of the initial energy. The series in Eq. (31) was calculated numerically for a simple equilibrium case. The calculations show that with an increasing number of ITE IMC steps the series does not converge and is greater than T. This means that the ITE IMC will not yield strictly positive material temperatures as both the time step size and number of ITE IMC steps is increased. This situation is highly unlikely because it assumes that none of the emitted energy is absorbed in the material during a time step. Negative temperatures were not encountered in any of the results in this paper; nevertheless this is a downside of the ITE IMC method.

3.2. Implementing the ITE IMC equations

An arbitrary number of sub-steps can be used in the ITE IMC method. If one step is used, the ITE IMC method becomes the standard IMC method. The main difference in implementation between ITE and IMC is the need to divide the emission energy and the initial census energy by the total number of sub-steps, N. After dividing by N, the simulation is performed just like a standard IMC simulation. At the end of the IMC simulation for each T_i, Eq. (27) is used to determine the sub-temperature at t^{n+1}. The equation for T_i^{n+1} for a given zone on the mesh is:

$$T_{j,i}^{n+1} = T_{j,i}^{n} + \frac{1}{c_V}\frac{[E_{abs}]}{\Delta x} - \frac{1}{N}\left(\frac{\Delta t}{c_{v,i}} f_i \sigma_{a,p,i} a c T_{i,N}^4\right), \tag{34}$$

where $T_{j,i}$ is the material temperature in a given zone j, $T_{i,N}$ is from Eq. (25) and $[E_{abs}]$ is the absorption tally from the IMC simulation. The absorption tally is the total energy absorbed in the zone and the energy density is obtained by dividing the tally by Δx (in more than one dimension it would be divided by the zone's volume). Eq. (25) is then recalculated for this zone and the emission source and the material properties are updated for the next sub-temperature calculation.

In ITE IMC, it is also necessary to keep a master list of census particles at the end of the time step from all sub-temperature calculations. After all ITE sub-steps have been completed, the master list is divided into N smaller lists using

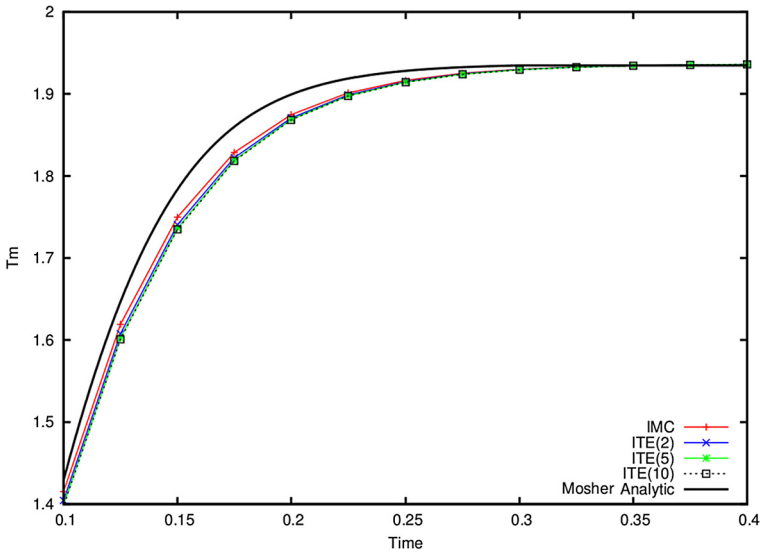

Fig. 1. Material temperature vs. time comparing IMC and ITE IMC to the analytic solution near the equilibrium temperature.

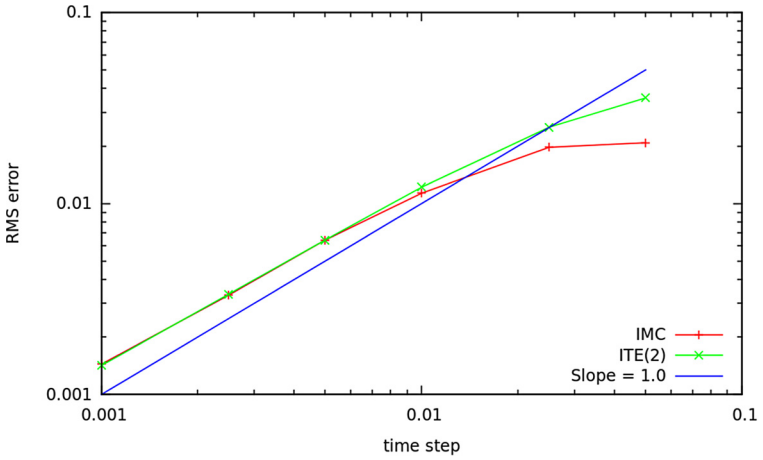

Fig. 2. The Root Mean Square (RMS) error vs. Δt of IMC and ITE IMC with 2 sub-steps compared to Mosher analytic.

pseudo-random numbers. These smaller lists then serve as the initial condition for each sub-step in the next time step. The shuffling procedure attempts to equalize the initial census energy for each sub-step material temperature calculation during a time step.

4. Results

To demonstrate that the ITE IMC method can accurately solve thermal radiative transfer problems and that the method has been correctly implemented in a computer code, we consider the results of several test problems.

4.1. Infinite medium

Mosher provided a time-dependent analytic solution to an infinite medium TRT problem with constant opacity and heat capacity [15]. A 1-D test problem with reflecting boundary conditions on both ends (an infinite medium) was simulated using the ITE IMC method. For the test problem the constants a and c, as well as the physical parameters σ and c_V, were set to 1.0, making the problem unitless. The initial radiation temperature T_r was set to 2.0 and the material temperature T_m was set to 0.001.

The results in Fig. 1 compare the IMC and ITE IMC method results to the analytic solution. Fig. 2 shows that the Root Mean Square (RMS) error approaches zero as the time step is decreased and that the IMC and ITE IMC method are both first order in time. Both the IMC and ITE IMC method obtain the correct equilibrium solution but have a lower material

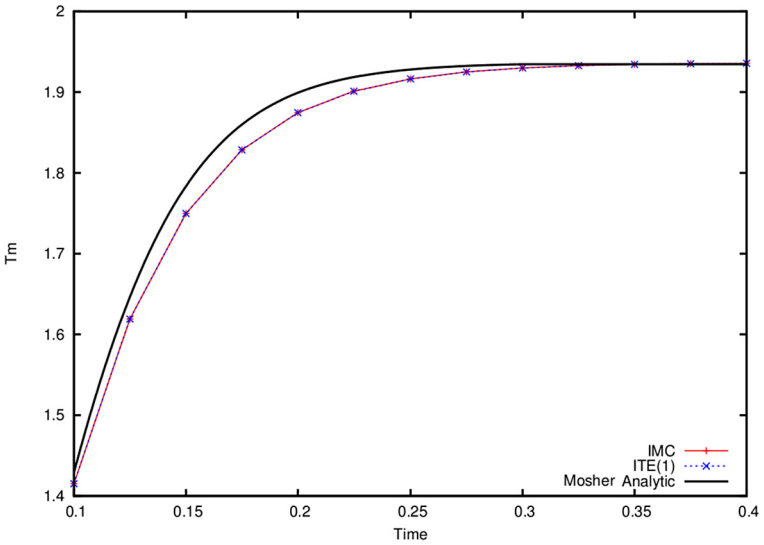

Fig. 3. Material temperature vs. time showing the equivalence of IMC and ITE IMC when 1 sub-step is used in the ITE method.

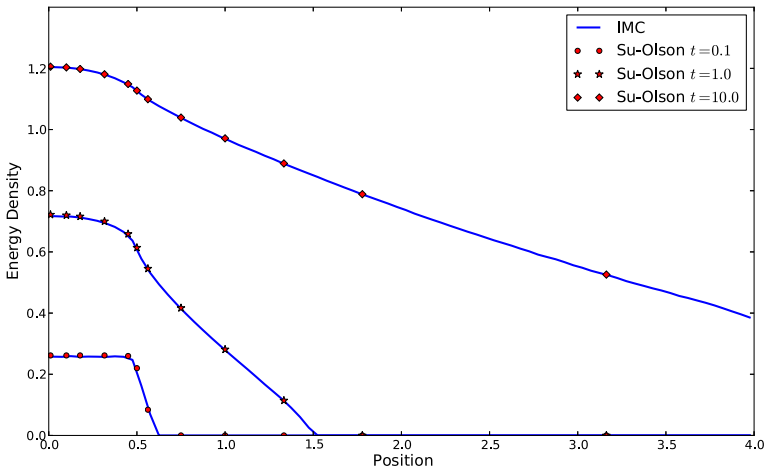

Fig. 4. Energy density vs. position comparing IMC to the analytic solution at various times.

temperature during the transient. Fig. 3 shows that the IMC and ITE IMC are equivalent when one sub-step is used in the ITE method.

4.2. 1-D

Su and Olson have developed test problems that are useful for verifying TRT codes. Their 1997 [16] paper provides the analytic solution for a one-dimensional, time-dependent, linear TRT problem. The TRT equations are linearized by assuming that the heat capacity is proportional to T_m^3, an approximation that was first used by Pomraning [17] and is very useful for obtaining reference solutions. This assumption is not physical, but it makes the TRT equations linear in T^4. Both the IMC and ITE IMC methods were used to simulate this test problem with $a = c = \sigma = 1.0$ and $c_V = 4.0T_m^3$. In the Su–Olson problem, a source of 1.0 (representing radiation coming from material at $T = 1.0$) located between $x = 0$ and $x = 0.5$ is present for 10.0 units of time and then turned off. The left boundary is reflecting and the right boundary is a vacuum. Figs. 4 and 5 show that the IMC method and the ITE IMC method agree with the analytic solution and with each other. Fig. 6 shows the RMS error for a run with zone centers that correspond to the x position where the Su–Olson analytic solution is available. The error does not decrease uniformly with smaller time steps due to the error also present from spatial discretization. If the spatial mesh is refined three times, the RMS error at $t = 10.0$ with $\Delta_t = 0.05$ is reduced to 7.95×10^{-3} for the IMC method and 6.82×10^{-3} for the ITE IMC method with four sub-steps. This refinement reduces the RMS error by a factor of two for the same time step size.

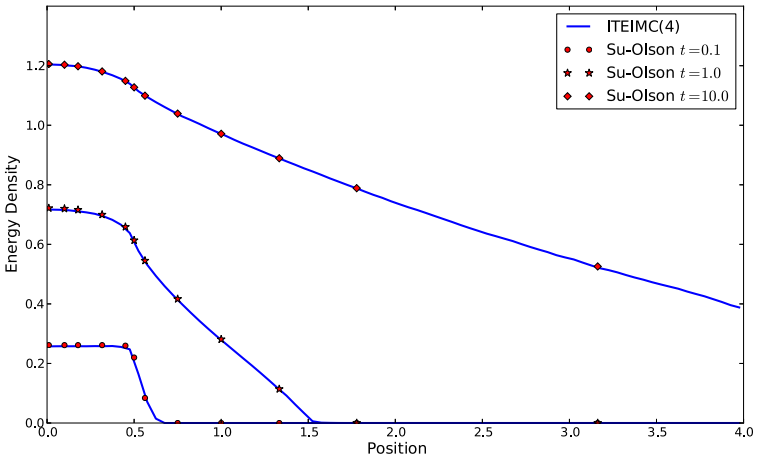

Fig. 5. Energy density vs. position comparing ITE IMC to the analytic solution at various times.

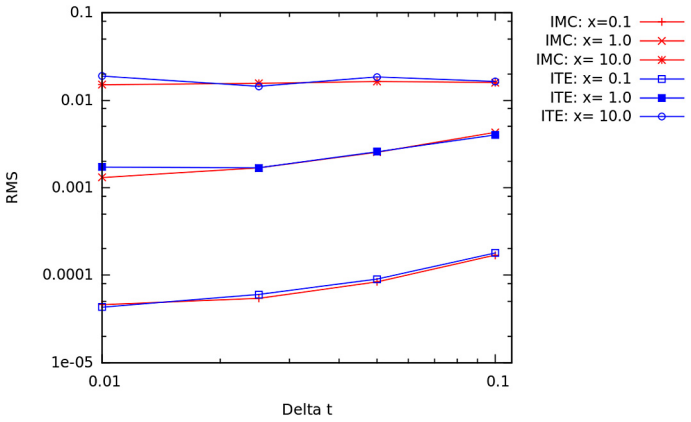

Fig. 6. Root Mean Square (RMS) time error vs. time step size, Δt, for the IMC and ITE IMC method with four sub-steps.

4.3. Stability analysis

Mosher and Densmore [13] evaluated the stability of the grey IMC equations in an infinite medium by again assuming that the heat capacity is proportional to T^3. The IMC equations then become a system of equations that can be solved exactly and analyzed by examining the solution at t_{n+1}: the radiation energy density E^{n+1} and the material energy density U^{n+1}. The method of stability analysis used by Mosher and Densmore is applied to the ITE IMC equations: the same assumptions are made and the equations are solved for each sub-step temperature and this information is used in determining the next sub-step temperature. The motivation for solving these equations is finding the eigenvalues of the 2×2 matrix that comes from solving the equations exactly and using a given time step Δt:

$$\begin{pmatrix} E^{n+1} \\ U^{n+1} \end{pmatrix} = \begin{pmatrix} a(\Delta t) & b(\Delta t) \\ c(\Delta t) & d(\Delta t) \end{pmatrix} \begin{pmatrix} E \\ U \end{pmatrix}. \tag{35}$$

The eigenvalues can then be used to determine the amplification factor for a given time step size Δt.

In this analysis, the opacity is independent of temperature and the equations are linearized by assuming that the material energy, U, is proportional to T^4:

$$U = bT^4. \tag{36}$$

This is equivalent to the linearization of Pomraning, where heat capacity is assumed to vary with T^3. The assumption in Eq. (36) yields a simple relationship between material energy and the equilibrium radiation density:

$$U_r = aT^4 = \frac{a}{b}U = \beta U. \tag{37}$$

The standard 0-D IMC equations are:

$$\frac{dE}{dt} + f_n\sigma_n cE = f_n\sigma_n cU_r^n, \tag{38}$$

$$\frac{dU}{dt} = f_n\sigma_n c\left(E - U_r^n\right). \tag{39}$$

A slight modification is made when using two steps of the ITE IMC method:

$$\frac{dE_1}{dt} + f_1^n\sigma^n cE_1 = f_1^n\sigma^n cU_{1,r}^{n+1}, \tag{40}$$

$$\frac{dU_1}{dt} = f_1^n\sigma^n c\left(E_1 - U_{1,r}^{n+1}\right). \tag{41}$$

In the ITE IMC method U_r^{n+1} is estimated using information from the previous sub-steps. For the first sub-step, the ITE IMC method estimates the emission temperature, $U_{r,1}^{n+1}$, with $U_{r,1}^{n+1} = \frac{U_r^n}{2}$. These equations can be solved and evaluated at t_{n+1} to yield:

$$E_1^{n+1} = \frac{1}{2}\left(E^n e^{-f_1^n\sigma^n c(t-t_n)} + U_r^n\left(1 - e^{-f_1^n\sigma^n c\Delta t}\right)\right), \tag{42}$$

$$U_1^{n+1} = \frac{1}{2}\left(U^n + \left(E^n - U_r^n\right)\left(1 - e^{-f_1^n\sigma^n c\Delta t)}\right)\right). \tag{43}$$

These equations can be written in a general form:

$$E_1^{n+1} = \frac{1}{2}AE^n + \frac{1}{2}BU^n, \tag{44}$$

$$U_1^{n+1} = \frac{1}{2}(1-A)E^n + \frac{1}{2}(1-B)U^n. \tag{45}$$

If two steps are used in the ITE IMC method, the emission temperature for the second sub-step is estimated as $U_{r,2}^{n+1} = \frac{U_{r,1}^{n+1} + U_{r,2}^n}{2}$ and $U_{r,2}^n = \frac{U_r^n}{2}$. The radiation transport and material energy balance equations for the second sub-step become

$$\frac{dE_2}{dt} + f_2^n\sigma^n cE_2 = f_2^n\sigma^n c\frac{U_{r,1}^{n+1} + \frac{U_r^n}{2}}{2}, \tag{46}$$

$$\frac{dU_2}{dt} = f_2^n\sigma^n c\left(E_2 - \frac{U_{r,1}^{n+1} + \frac{U_r^n}{2}}{2}\right), \tag{47}$$

where $U_{1,r}^{n+1}$ is now a constant equal to $\beta U_1(t_{n+1})$.

This system of equations is then solved to yield an expression for E_2^{n+1} and U_2^{n+1}:

$$E_2^{n+1} = \left(\frac{1}{2}\gamma_2 + U_{1,E}\left(\frac{1}{2}\beta - \frac{1}{2}\beta\gamma_2\right)\right)E + \left(\frac{1}{4}\beta - \frac{1}{4}\beta\gamma_2 + U_{1,U}\left(\frac{1}{2}\beta - \frac{1}{2}\beta\gamma_2\right)\right)U, \tag{48}$$

$$U_2^{n+1} = \left(\frac{1}{2} - \frac{1}{2}\gamma_2 - U_{1,E}\left(\frac{1}{2}\beta - \frac{1}{2}\beta\gamma_2\right)\right)E + \left(\frac{1}{2} - \frac{1}{4}\beta + \frac{1}{4}\beta\gamma_2 - U_{1,U}\left(\frac{1}{2}\beta - \frac{1}{2}\beta\gamma_2\right)\right)U. \tag{49}$$

Because the equations are linearized, β is constant:

$$\beta = \frac{dU_r}{dU} = \frac{a}{b}. \tag{50}$$

In Eqs. (48) and (49), $\alpha = -f^n\sigma^n c$ and $\gamma = e^{-\alpha\Delta t}$. β is used to eliminate U_r in favor of U. Eqs. (48) and (49) can also be rewritten in a general form:

$$E_2^{n+1} = \frac{1}{2}A'E^n + \frac{1}{2}B'U^n, \tag{51}$$

$$U_2^{n+1} = \frac{1}{2}\left(1 - A'\right)E^n + \frac{1}{2}\left(1 - B'\right)U^n. \tag{52}$$

If more than two sub-steps are used in ITE IMC, the equations for any sub-step can be written in the same general form because the U_r term for any sub-step U_i with $i > 1$ is simply U_i plus the previously determined U_r^{n+1} terms, which are known:

$$U_{r,i} = U_i + \sum_{j=1}^{i-1} U_{r,j}^{n+1}, \tag{53}$$

where j is an ITE sub-step that has already been determined and i corresponds to the current sub-step.

U^{n+1} and E^{n+1} are determined by summing the values for U_i^{n+1} and E_i^{n+1} over all the sub-steps. Using the general forms of those equations yields

$$E^{n+1} = \left(A + A'\right)E^n + \left(B + B'\right)U^n, \tag{54}$$

$$U^{n+1} = \left((1-A) + \left(1-A'\right)\right)E^n + \left((1-B) + \left(1-B'\right)\right)E^n. \tag{55}$$

This system of equations again simplifies to the form:

$$E^{n+1} = CE^n + DU^n, \tag{56}$$

$$U^{n+1} = (1-C)E^n + (1-D)U^n. \tag{57}$$

Any 2×2 system of equations of this form will have the same eigenvalues:

$$\lambda_1 = 1, \qquad \lambda_2 = C - D. \tag{58}$$

The stability can then be determined such that $|C - D|$ is maintained less than unity. The ITE method for an arbitrary number of steps results in an equation like Eqs. (56) and (57), and thus the ITE method eigenvalues always have the same form.

An expression for $|C - D|$ can be determined for any number of sub-steps when using the ITE method in 0-D. Consider sub-step i of an ITE method with N sub-steps:

$$\frac{dE_i}{dt} + f_i^n \sigma^n c E_i = f_i^n \sigma^n c U_{r,i}^{n+1}, \tag{59}$$

$$\frac{dU_i}{dt} = f_i^n \sigma^n c\left(E_i - U_{r,i}^{n+1}\right), \tag{60}$$

where $U_{r,i}^{n+1}$ is now a function of all the previous time steps:

$$U_{r,i}^{n+1} = \frac{U_{r,1}^{n+1} + U_{r,2}^{n+1} + \ldots + U_{r,i-1}^{n+1} + \frac{(N-i)U_r^n}{N}}{N}. \tag{61}$$

The equations for E_i^{n+1} and U_i^{n+1} are:

$$E_i^{n+1} = \left(\frac{1}{N}\gamma_i + U_{C,E}\left(\frac{1}{N}\beta - \frac{1}{N}\beta\gamma_i\right)\right)E + \left(\frac{N-i+1}{N^2}\beta - \frac{N-i+1}{N^2}\beta\gamma_i + U_{C,U}\left(\frac{1}{N}\beta - \frac{1}{N}\beta\gamma_i\right)\right)U, \tag{62}$$

$$U_i^{n+1} = \left(\frac{1}{N} - \left(\frac{1}{N}\gamma_i + U_{C,E}\left(\frac{1}{N}\beta - \frac{1}{N}\beta\gamma_i\right)\right)\right)E + \left(\frac{1}{N} - \left(\frac{N-i+1}{N^2}\beta - \frac{N-i+1}{N^2}\beta\gamma_i + U_{C,U}\left(\frac{1}{N}\beta - \frac{1}{N}\beta\gamma_i\right)\right)\right)U, \tag{63}$$

where

$$U_{C,E} = U_{1,E} + U_{2,E} + \ldots + U_{i-1,E}, \tag{64}$$

and

$$U_{C,U} = U_{1,U} + U_{2,U} + \ldots + U_{i-1,U}. \tag{65}$$

These U_C values represent the coefficients in front of E and U in each U_i equation (E_i equations are only used when calculating the total E^{n+1}). The $N - i + 1$ terms come from the addition of the $U_{i+1} \ldots U_N$ values that have not yet been determined and are thus approximated as $\frac{U_r^n}{N}$. Because U_i and E_i depend on all the previous sub-steps, Eqs. (62) and (63) can be used recursively to find the numerical values of the coefficients for U_i and E_i. When $i = 1$, Eqs. (42) and (43) are used to calculate the coefficients. The stability of the system is determined from $|C - D| < 1$ where C and D are:

$$C = (E_{1,E} + E_{2,E} + \ldots + E_{N-1,E} + E_{N,E}), \tag{66}$$

$$D = (E_{1,U} + E_{2,U} + \ldots + E_{N-1,U} + E_{N,U}), \tag{67}$$

where $E_{i,E}$ and $E_{i,U}$ are coefficients multiplying the respective E and U terms in the E_i^{n+1} equation. Although this stability analysis has been performed for a linear problem, other work has been done to show how this specific linear problem relates to the stability of non-linear problems [18,19].

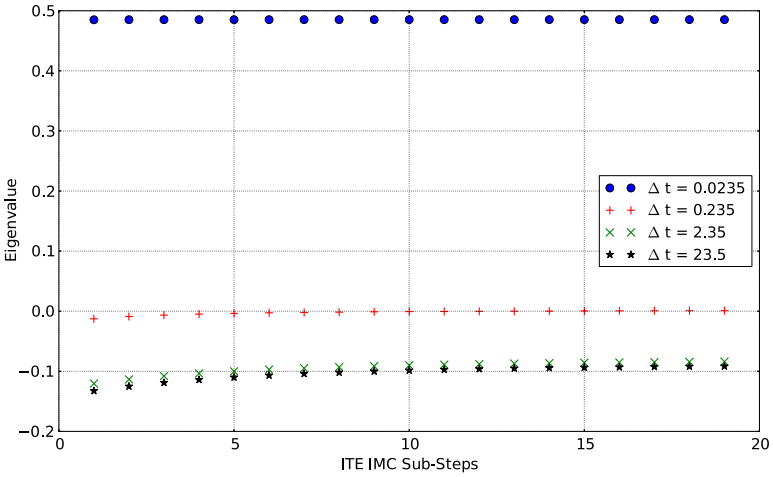

Fig. 7. λ_2 values vs. ITE IMC steps for various Δt values.

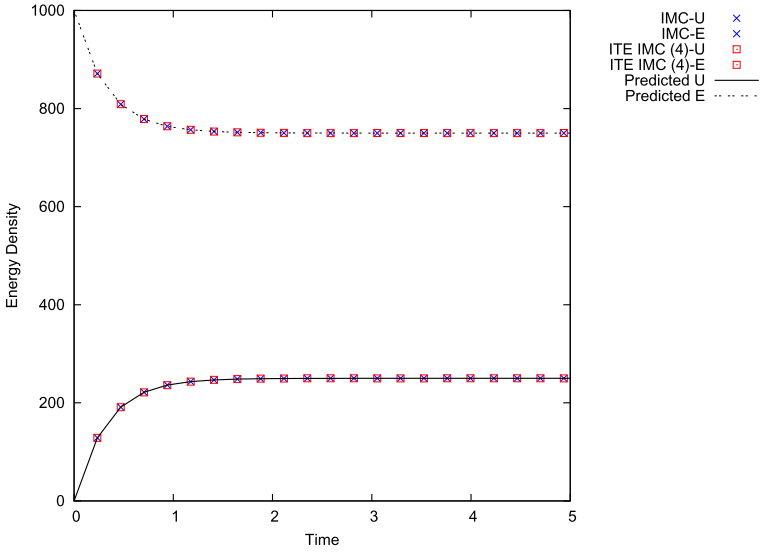

Fig. 8. Radiative and material energy density vs. time for $\Delta t = 0.235$.

4.4. Stability analysis numerical results

The second eigenvalue, λ_2, was numerically calculated with $a = c = 1$, $\sigma = 10.0$ and $\beta = 3$ for various values of Δt. The results are shown in Fig. 7. For all values of Δt, $|\lambda_2| < 1$ and for $\Delta t < 2.1$ the solution is monotonic ($0 < \lambda_2 < 1$). If enough sub-steps are used, The ITE IMC method is monotonic over a slightly larger range than the standard IMC method as seen in Fig. 7. For time steps greater than 2.1, the eigenvalue decreases slightly as more ITE sub-steps are used. IMC and ITE IMC simulations were performed with $a = c = \sigma = 1$ for $\Delta t = 0.235$ and $\Delta t = 50.0$ with an initial radiation density $E_0 = 1000$ and an initial material energy density $U_0 = 0.0$. Figs. 8–10 show E and U as a function of time. Fig. 8 shows that for positive eigenvalues, IMC and ITE IMC generate solutions that compare very well with the predicted solution and with each other (they have the same λ_2). For $\Delta t = 50.0$ in Fig. 9, the IMC and ITE IMC simulation values again compare well with the predicted values. In Fig. 10, the smaller predicted λ_2 value for the ITE IMC method with four sub-steps is evident in the slightly less oscillatory nature of the solution.

4.5. Crooked pipe problem

The crooked pipe test problem was designed by Graziani and LeBlanc in 2000 [20]. Its purpose is to test the validity of radiation transport codes in non-diffusive conditions. In the crooked pipe problem, there are two material regions: an optically thin region with a lower heat capacity and an optically thick region with a high heat capacity. The thin region is the pipe and it is embedded within the thick material. The problem described by Graziani and LeBlanc is solved in curvilinear

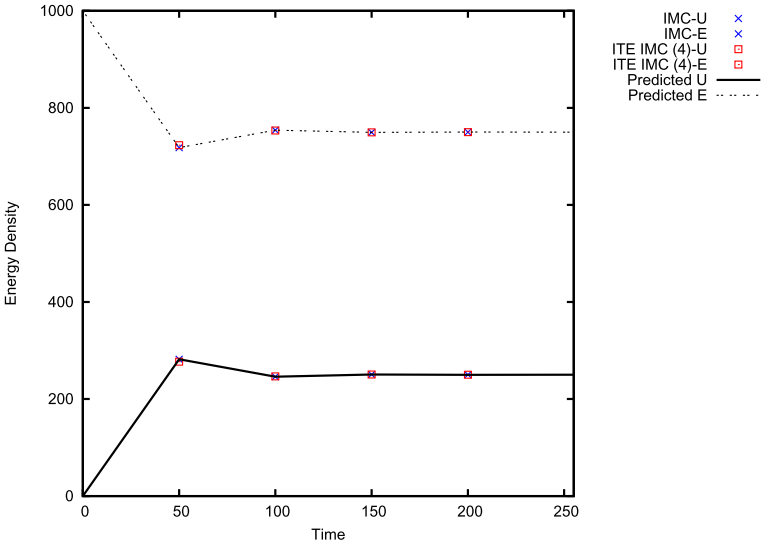

Fig. 9. Radiative and material energy density vs. time for $\Delta t = 50.0$.

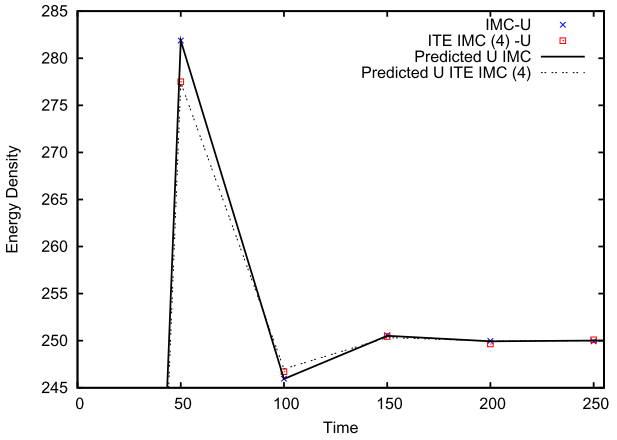

Fig. 10. Material energy density vs. time for IMC and ITE IMC with 4 sub-steps.

Table 1
Physical parameters for the crooked pipe test problem.

σ_{thick}	=	2000 cm^{-1}
σ_{thin}	=	0.2 cm^{-1}
$c_{V\,thick}$	=	10^{15} $\frac{\text{erg}}{\text{keV cm}^3}$
$c_{V\,thin}$	=	10^{12} $\frac{\text{erg}}{\text{keV cm}^3}$
T_0	=	0.05 keV
T_B	=	0.5 keV
Δt	=	0.0001 ns
Photons	=	400 000
c	=	30.0 $\frac{\text{cm}}{\text{ns}}$
a	=	1.3720160×10^{14} $\frac{\text{erg}}{\text{cm}^3\,\text{keV}^4}$

r–z geometry. The pipe has four 90 degree turns as it runs from $z = 0$ to $r = 7.0$ cm. We expect to see shadowing at these corners until the walls of the pipe heat up. In the diffusion approximation the current is proportional to the gradient of the intensity. This means that radiation would be transported into these "shadowed" regions resulting in faster transport of energy. In an optically thick, highly scattering medium, diffusion theory is valid, but it is not in optically thin regions. A 0.5 keV source is placed at $z = 0$ and vacuum boundaries are imposed at $z = 0$, $r = 2.0$ cm and $z = 7.0$ cm. We impose a reflecting boundary at $r = 0$. Other parameters are shown in Table 1.

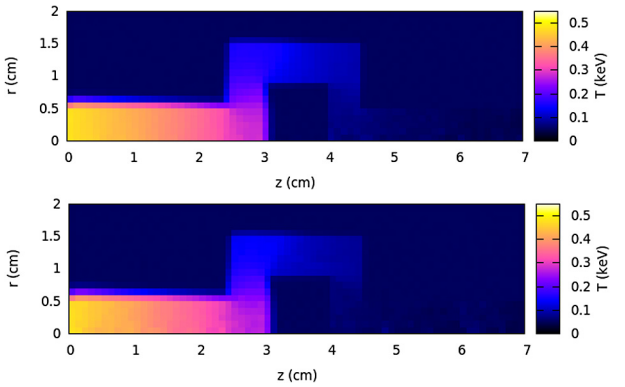

Fig. 11. Material temperature vs. position at $t = 175$ ns for IMC (top) and ITE IMC(4) (bottom).

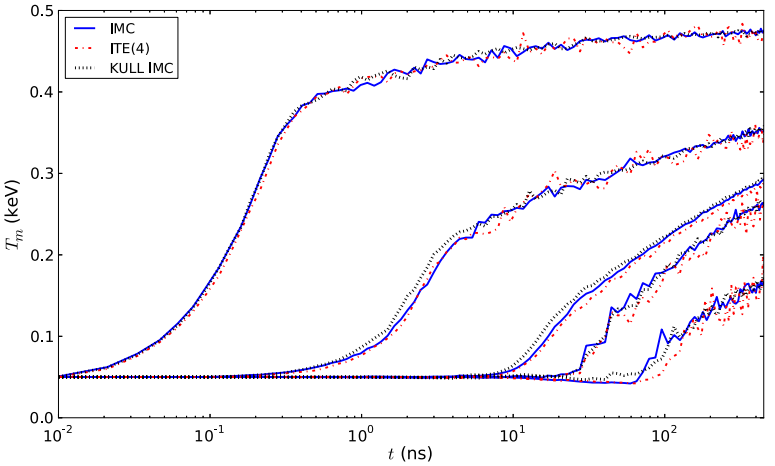

Fig. 12. Material temperature vs. time for the five examined points in crooked pipe problem.

The temperature is plotted at 5 points within the "pipe": Point 1: $z = 0.25$ cm, $r = 0$, Point 2: $z = 2.75$ cm, $r = 0$, Point 3: $z = 3.5$ cm, $r = 1.25$ cm, Point 4: $z = 4.25$ cm, $r = 0$, and Point 5: $z = 6.75$ cm, $r = 0$ cm.

In Fig. 11 heat maps of the IMC and ITE IMC results at 1.75 ns are compared side by side. Fig. 12 shows the temperature at the 5 points as a function of time for the IMC and ITE IMC methods. The larger variance with time is expected, because as more energy enters the problem, the same number of particles are used to simulate that energy, so each zone on the mesh will receive fewer particles. Fig. 12 demonstrates a rough agreement between IMC and ITE IMC in the crooked pipe problem. Fig. 12 also contains the crooked pipe results for the IMC package inside the KULL [21] multiphysics code for the purpose of showing agreement between the author's personal IMC code and a widely used IMC implementation. The KULL IMC code was run without any teleportation error correction algorithm so it could be compared directly to the author's IMC code. The large variance in material temperature present in the ITE IMC method is visible in Fig. 11. The ITE IMC temperature slightly lags behind the IMC solution, possibly because the ITE IMC method is more prone to teleportation error. This is because the emission temperatures change within a time step for the ITE IMC method. This gives rise to more energy being transported into the thick regions in the crooked pipe problem and a lagging wavefront.

4.6. 0-D non-linear opacity

Gentile gave the analytic solution for a 0-D test problem where opacity is proportional to T^{-5} [9]. This problem was run with the parameters in Table 2.

The initial radiation temperature was chosen so that at equilibrium the material temperature will be 1.0 keV. This problem is highly non-linear due to the temperature dependent opacity. The opacity ranges from 1.0×10^7 cm^{-1} at $t = 0.0$ to 1.0×10^{-3} cm^{-1} at equilibrium. The results in Fig. 13 show the IMC results compared to the analytic solution. The IMC method does obtain the equilibrium solution but both the material temperature and radiation temperature are incorrect in the transient. The IMC method produces material temperatures above 1 keV that then cool to equilibrium unless the time step is less than about 1.0×10^{-18} s. Material temperatures higher than the initial thermal temperatures are a violation of the maximum principle. Fig. 14 shows that the ITE IMC method does not violate the maximum principle and converges to the analytic solution as the number of sub-steps is increased. The additional lines on Fig. 14 for a given number of ITE

Table 2
Physical parameters for 0-D non-linear opacity test problems.

$\sigma_a(T)$	$=$	$\frac{1.0\times10^{-3}}{T^5}$
c_V	$=$	$5\times10^{14}\ \frac{\text{erg}}{\text{keV}}\ \text{cm}^3$
$T_{m,0}$	$=$	0.01 keV
$T_{r,0}$	$=$	1.46512 keV
c	$=$	$30.0\ \frac{\text{cm}}{\text{ns}}$
a	$=$	$1.3720160\times10^{14}\ \frac{\text{erg}}{\text{cm}^3\ \text{keV}^4}$

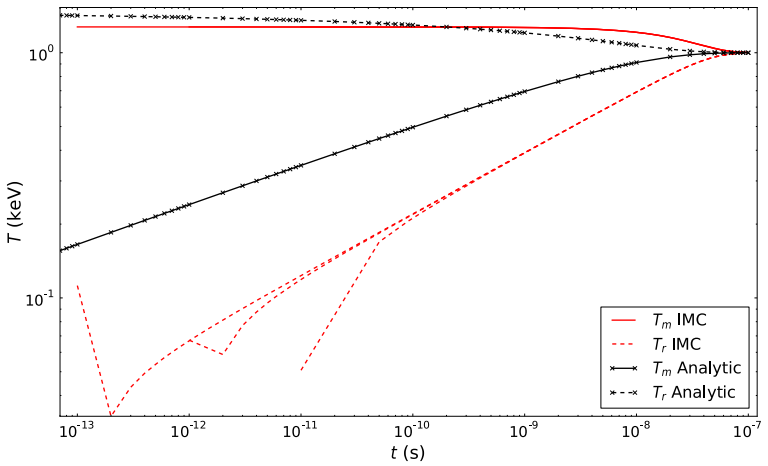

Fig. 13. Material temperature vs. time for the 0-D non-linear opacity problem using the IMC method with various time step sizes.

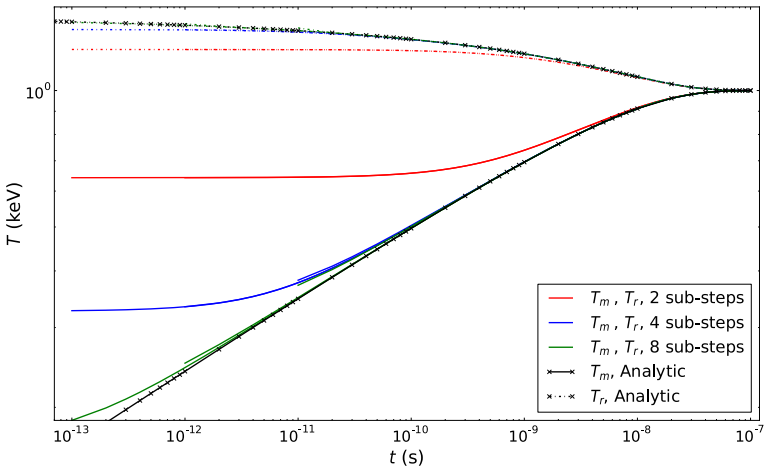

Fig. 14. Material temperature vs. time for the 0-D non-linear opacity problem using the ITE IMC method with various time step sizes.

sub-steps are for different time step sizes. For comparison, when using 8 sub-steps with the ITE IMC method the correct behavior can be obtained with a time step size about 1.0×10^6 times larger than the IMC method.

4.7. Marshak wave

The ITE IMC method is especially effective in Marshak wave problems, where violations of the maximum principle are likely to occur. The Marshak wave problem from Larsen and Mercier's paper [5] was simulated with both IMC and ITE IMC methods. In the Marshak wave problem, the opacity is proportional to $\frac{1}{T^3}$, meaning that cold regions will have a very small mean free path. A boundary source, $T_B = 1.0$ keV, emits photons that heat the relatively cold matter ($T_0 =$ 0.001 keV) inside the problem. As the material heats up it becomes more transparent to photons. The IMC method does not update its temperature-dependent properties during the time step, so the cold material will be very opaque throughout the time step, and too much energy will be absorbed if the time step is relatively large. The ITE IMC method updates the

Table 3
Physical parameters for Marshak wave test problems.

$\sigma_a(T)$	$=$	$\frac{15}{\pi^4}\frac{27}{T^3}$
c_V	$=$	8.1181×10^{13} $\frac{\text{erg}}{\text{keV cm}^3}$
T_0	$=$	0.001 keV
T_B	$=$	1.0 keV
c	$=$	30.0 $\frac{\text{cm}}{\text{ns}}$
a	$=$	1.3720160e14 $\frac{\text{erg}}{\text{cm}^3\ \text{keV}^4}$

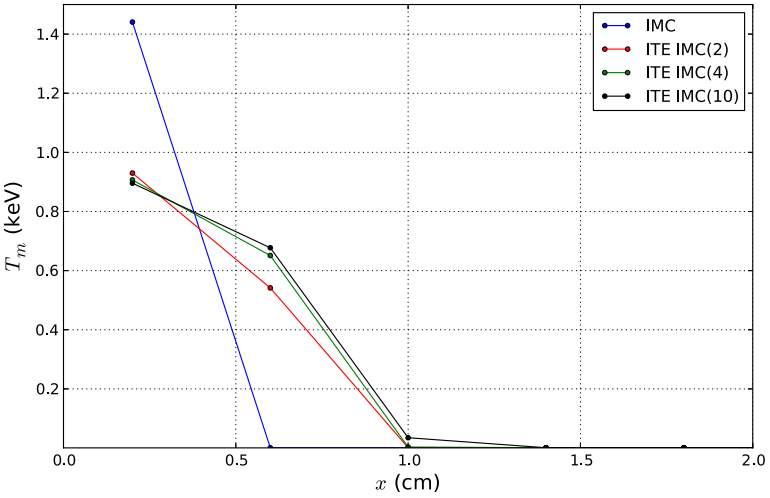

Fig. 15. Material temperature vs. position at the end of one time step where $\Delta t = 0.4$ ns and $\Delta x = 0.4$ cm.

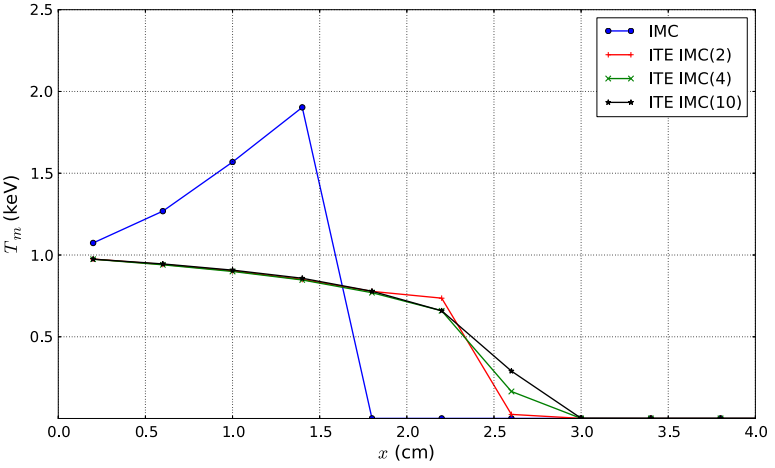

Fig. 16. Material temperature vs. position after at $t = 3.2$ ns, where $\Delta t = 0.8$ ns and $\Delta x = 0.4$ cm.

temperature-dependent properties at the end of each sub-step, thus allowing the material to become more transparent throughout the time step. If the internal material temperature is ever greater than the boundary temperature then the method is said to violate the maximum principle for that choice of grid spacing and time step.

The IMC and ITE IMC simulations used the physical parameters and boundary conditions from Table 3. Results at various times in the problem are shown in Figs. 15 and 16. Both figures show that the ITE IMC method allows more energy to enter the problem while maintaining all material temperatures below the boundary temperature. The figures also show that using more ITE IMC sub-steps allows more energy to penetrate further into the problem. In this case more energy penetration is correct because as a zone heats up energy can pass through. In the IMC method the cold, thick zone at the wavefront stays cold and thick throughout the time step.

A script was developed to determine the conditions under which IMC and ITE IMC first violate the maximum principle: the Marshak wave problem was simulated with constant grid spacing and a small time step. The time step was gradually

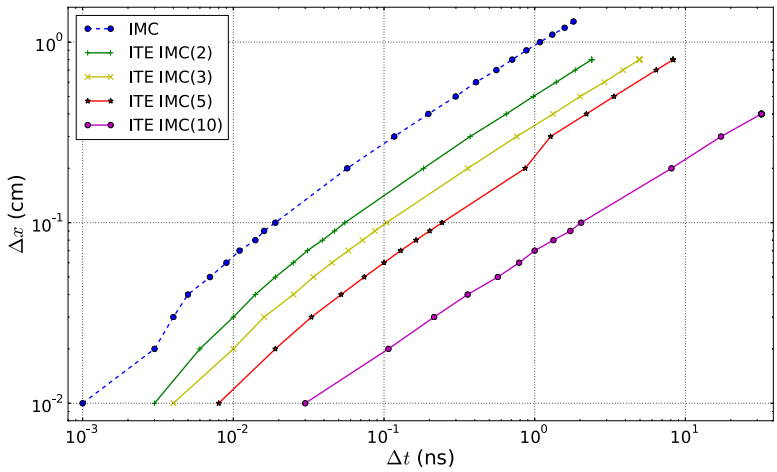

Fig. 17. First violations of the maximum principle for Standard IMC and the ITE IMC method.

increased until a violation of the maximum principle occurred. This procedure was used to generate the data in Fig. 17, which shows that the ITE IMC method always allows for larger time steps without violating the maximum principle for any level of grid spacing. The relationship between allowable time step size and number of ITE sub-steps is non-linear: doubling the number of sub-steps from 5 to 10 always increases the allowable time step size by more than a factor of 2.0.

The reduction in the maximum principle violation for ITE IMC vs. IMC is much more obvious for the Marshak wave test problem than it is in the linear analysis. We wish to emphasize that violations of the maximum principle are not the result of numerical instability. The IMC equations are stable: violations of the maximum principle are transient in time, and IMC yields the correct equilibrium result. The violations of the maximum principle result from a lack of full implicitness in IMC. As mentioned in the text following Eq. (14), IMC is semi-implicit; it does not iterate to obtain consistent t^{n+1} values of the material temperature. ITE IMC is less prone to produce violations of the maximum principle because later sub-steps use an emission temperature that is a more accurate approximation of T^{n+1}, because they use information on the matter temperature gained from earlier sub-steps.

4.7.1. Teleportation error

The teleportation error associated with ITE IMC method was determined using the method of Cheatham [6]. This test problem is grey and 1D with $c_V = 4.0T^3$, $a = c = 1.0$ (the problem is unitless) and $\sigma = 100.0$. Vacuum boundary conditions are imposed on both sides and a plane source of 1.0 is placed at the left boundary. The results are compared at $t = 10.0$ with an IMC simulation that used $\Delta x = 0.01$ and $\Delta t = 0.05$. To investigate the behavior of the teleportation error, Δx is increased relative to the reference solution or Δt is decreased. Fig. 18 shows how energy is transferred further into the problem as Δt is decreased. The ITE IMC method has a higher material temperature relative to the reference solution. Photon teleportation results because the emission location of a particle is sampled uniformly over a zone. Effective scattering reduces the amount of teleportation error, because it reduces the amount of thermal emission. A fraction of the thermal emission is replaced by effective scatters, which occur at the "correct" location instead of at an inaccurately estimated emission location. The ITE IMC method emits particles multiple times during a time step, with a Fleck factor that decreases with each sub-step. This means that uniform position sampling occurs more frequently in ITE IMC during a time step than in IMC. Fig. 19 compares the teleportation error for different numbers of ITE IMC sub-steps. As the number of sub-steps is increased, the overheating due to teleportation also increases. The teleportation error does not increase indefinitely as ITE IMC sub-steps are increased. This is likely because at some point the amount of effective scattering is negligible, so all thermal emission occurs at estimated positions.

4.8. Variance

The figure of merit (FOM) for Monte Carlo problems is defined as the reciprocal of the product of the variance of the result and the run time:

$$FOM = \frac{1}{t\sigma^2}, \tag{68}$$

where σ^2 is the variance of the answer (usually the material or radiation temperature) and t is the run time. Shorter run times and smaller variances yield a larger FOM.

For non-linear Monte Carlo problems, a simple relationship cannot be used to determine the variance. Instead, we draw an analogue to the variance of the solution by looking at the L^1 error norm in infinite medium problems at equilibrium. The IMC and ITE IMC methods both hold the equilibrium solution, so the error in the equilibrium solution can be attributed to

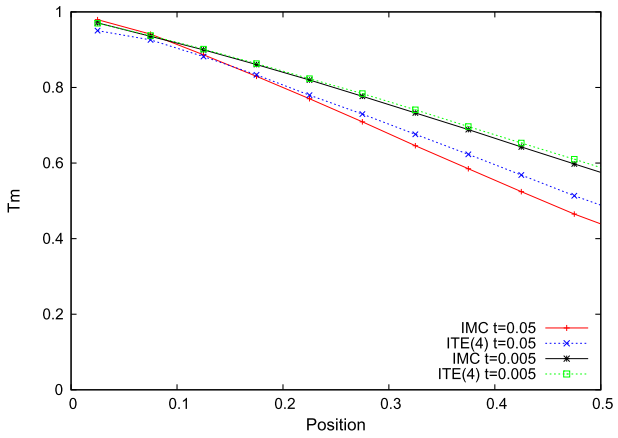

Fig. 18. Material temperature vs. position in teleportation problem for IMC and ITE IMC at $t = 10.0$.

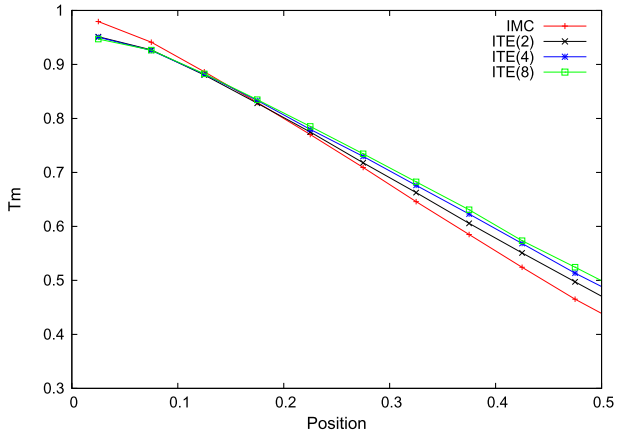

Fig. 19. Material temperature vs. position for $\Delta t = 0.05$ at $t = 10.0$ for the ITE IMC method with varying number of sub-steps.

the Monte Carlo noise associated with each method. The error after one time step for a problems at equilibrium for the IMC method and the ITE IMC method with four sub-steps is shown in Fig. 20. Here the error is shown for various equilibrium temperatures. For large temperatures, the error is larger for the ITE IMC method. For low equilibrium temperatures, the error in both methods is comparable. This discrepancy between the variance in the IMC and ITE IMC methods can be explained by the different Fleck factors used in each method. The IMC method uses the same Fleck factor throughout the time step. The ITE IMC method uses a different Fleck factor for each sub-step, as shown in Eq. (26). When the temperature term in the denominator of the Fleck factor is small, the Fleck factor does not change much between ITE IMC sub-steps. When the temperature is large, the $\frac{N-i+1}{N}$ term in Eq. (26) yields very different Fleck factors for each sub-step. Variance is related to the difference between the average event and individual events. Calculating the absorbed energy with differing Fleck factors will yield a wider range of individual events and thus more variance. When the Fleck factor is small ($\Delta t\sigma\beta \gg 1$), the ITE IMC method will have a wider range of Fleck factors for each sub-step and thus produce a solution with more variance. The larger variance when the Fleck factor is relatively small should be considered when using the ITE IMC method for a specific application. An example of this variance is shown in Fig. 21, where the IMC and ITE IMC solution are compared for an infinite medium problem at an equilibrium temperature of $T_m = 2.0$ keV.

The time to solution for the IMC and ITE IMC method is highly dependent on the temperature, which determines the amount of relative scattering through the Fleck factor. Because the ITE IMC method updates the temperature during a time step, the runtime will vary in an unpredictable way relative to the IMC method. If the temperatures are similar for the ITE IMC and standard IMC methods during a time step, the ITE IMC method can be expected to have a smaller FOM.

5. Conclusions

The ITE IMC method has been shown to satisfy the maximum principle for a wider range of problem parameters than standard IMC. The ITE IMC method has been validated in 0-D, 1-D and 2-D problems and with linear and non-linear problem parameters. The ITE IMC method shows considerable improvement for the highly non-linear opacity problem. The teleportation problem present in IMC simulations is exacerbated with the use of ITE IMC.

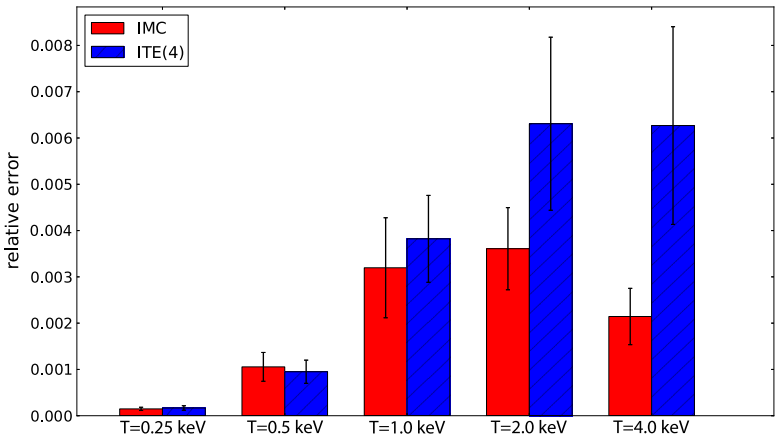

Fig. 20. Relative error vs. equilibrium temperature for IMC and ITE IMC for an infinite medium problem.

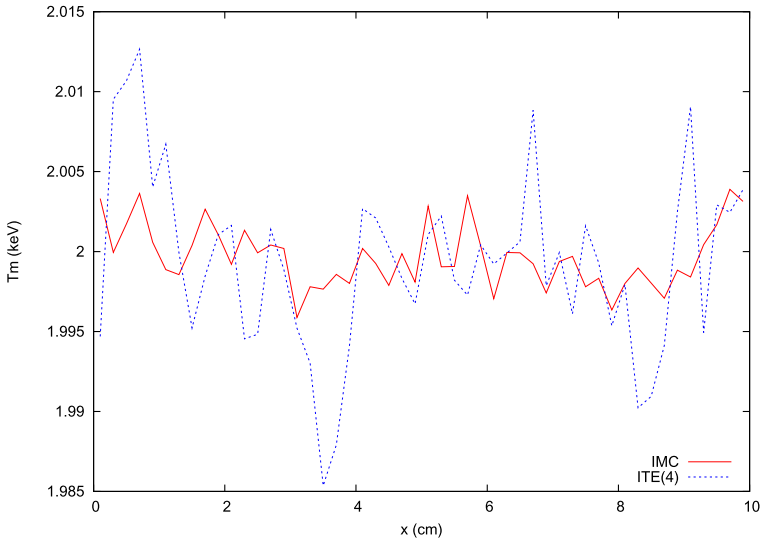

Fig. 21. Material temperature vs. position for IMC and ITE IMC in an infinite medium problem at equilibrium.

To evaluate the results, the ITE IMC method is compared with traditional IMC. The ITE IMC method presents one possible solution to the overheating problem present in IMC simulations. By using more sub-steps of the ITE IMC method, the simulation can be performed using larger time steps without violating the maximum principle, and the end result can be obtained more quickly. Currently, the variance of the ITE IMC solution will be larger than the IMC solution when the Fleck factor is small and the same number of particles are used for both methods. The source of this increased variance is the differing Fleck factors used within a time step in the ITE IMC method. For the test problem with highly non-linear opacity, the ITE IMC method can obtain a more accurate solution by increasing the number of sub-steps and shows dramatic improvement over the standard IMC solution. In problems where large zones are used, the teleportation error is larger when ITE IMC is used. The teleportation error increases when more ITE sub-steps are used.

The ITE IMC method can be used to reduce overall simulation time by allowing longer time steps without violating the maximum principle. The reduced run time comes at the cost of an increase in variance relative to the IMC method. Work on variance reduction and mitigation of teleportation error with ITE IMC is needed. Variance reduction techniques like global weight windows [7] or symbolic weights [22] could potentially be used with the ITE IMC method to reduce variance. Standard corrections for teleportation error could be implemented in ITE IMC and compared to standard IMC with the same methods.

ITE IMC provides a larger stability envelope for Marshak wave problems. We are currently working to characterize the time step limits on other common TRT problems.

References

[1] J.P. Apruzese, J.L. Giuliani, Multi-dimensional radiation transport for modeling axisymmetric Z pinches: ray tracing compared to Monte Carlo solutions for a two-level atom, J. Quant. Spectrosc. Radiat. Transf. 111 (1) (2010) 134–143.
[2] E.I. Moses, The National Ignition Facility (NIF): a path to fusion energy, in: iCENES'2007, 13th International Conference on Emerging Nuclear Energy Systems, June 3–8, 2007, Istanbul, Turkey, Energy Convers. Manag. 49 (7) (2008) 1795–1802.
[3] G. Scheffknecht, L. Al-Makhadmeh, U. Schnell, J. Maier, Oxy-fuel coal combustion—a review of the current state-of-the-art, Int. J. Greenh. Gas Control 5 (Supplement 1) (2011) S16–S35.
[4] J.A. Fleck, J.D. Cummings, An implicit Monte Carlo scheme for calculating time and frequency dependent nonlinear radiation transport, J. Comput. Phys. 8 (1971) 313–342.
[5] E.W. Larsen, B. Mercier, Analysis of a Monte Carlo method for nonlinear radiative transfer, J. Comput. Phys. 71 (1987) 50–64.
[6] J.R. Cheatham, Truncation analysis and numerical method improvements for the thermal radiative transfer equations, Ph.D. thesis, University of Michigan, Ann Arbor, Michigan, 2010.
[7] A.B. Wollaber, Advanced Monte Carlo methods for thermal radiation transport, Ph.D. thesis, University of Michigan, Ann Arbor, Michigan, 2008.
[8] R.G. McClarren, T.J. Urbatsch, A modified implicit Monte Carlo method for time-dependent radiative transfer with adaptive material coupling, J. Comput. Phys. 228 (16) (2009) 5669–5686.
[9] N.A. Gentile, Including the effects of temperature-dependent opacities in the implicit Monte Carlo algorithm, J. Comput. Phys. 230 (12) (2011) 5100–5114.
[10] A.B. Wollaber, E.W. Larsen, J.D. Densmore, Towards a frequency-dependent discrete maximum principle for the implicit Monte Carlo equations, in: Proc. of ANS M&C 2011, Rio de Janeiro, RJ, Brazil, May 8–12, 2011.
[11] H.H. Rosenbrock, Some general implicit processes for the numerical solution of differential equations, Comput. J. 5 (1963) 329–330.
[12] W.H. Press, S.A. Teukolsky, W.T. Vetterling, B.P. Flannery, Numerical Recipes: The Art of Scientific Computing, 3rd edition, Cambridge University Press, New York, 2007.
[13] S.W. Mosher, J.D. Densmore, Stability and monotonicity conditions for linear, grey, 0-d implicit Monte Carlo calculations, Trans. Am. Nucl. Soc. 93 (2005) 520–522.
[14] R.G. McClarren, T.J. Urbatsch, An implicit Monte Carlo method based on BDF-2 time integration for simulating nonlinear radiative transfer, Trans. Am. Nucl. Soc. 107 (2012) 502–505.
[15] S.W. Mosher, Exact solution of a nonlinear, time-dependent, infinite-medium, grey radiative transfer problem, Trans. Am. Nucl. Soc. 95 (2006) 744–747.
[16] B. Su, G.L. Olson, An analytical benchmark for non-equilibrium radiative transfer in an isotropically scattering medium, Ann. Nucl. Energy 24 (13) (1997) 1035–1055.
[17] G.C. Pomraning, The non-equilibrium Marshak wave problem, J. Quant. Spectrosc. Radiat. Transf. 21 (3) (1979) 249–261.
[18] E.W. Larsen, J.D. Densmore, A linearized theory for near-equilibrium thermal radiative transfer problems, in: Nuclear Mathematical and Computational Sciences: A Century in Review, A Century Anew, Gatlinburg, Tennessee, USA, April 6–11, 2003.
[19] A.B. Wollaber, E.W. Larsen, A linear stability analysis for nonlinear, grey, thermal radiative transfer problems, J. Comput. Phys. 230 (4) (2011) 1528–1546.
[20] F. Graziani, J. LeBlanc, The crooked pipe test problem, Tech. Rep. UCRL-MI-143393, 100, Lawrence Livermore National Laboratory, 2000.
[21] N.A. Gentile, N. Keen, J. Rathkopf, The KULL IMC package, Tech. Rep. UCRL-JC-132743, 100, Lawrence Livermore National Laboratory, 1998.
[22] E.D. Brooks, Symbolic implicit Monte Carlo, J. Comput. Phys. 83 (2) (1989) 433–446.